Engineering Science and Technology, an International Journal 33 (2022) 101069

HOSTED BY

Contents lists available at ScienceDirect

Engineering Science and Technology, an International Journal

journal homepage: www.elsevier.com/locate/jestch

Full Length Article

An effective analog circuit design of approximate fractional-order derivative models of M-SBL fitting method

Murat Koseoglu [a], Furkan Nur Deniz [a,*], Baris Baykant Alagoz [b], Hafiz Alisoy [c]

[a] Inonu University, Department of Electrical and Electronics Engineering, Malatya, Turkey
[b] Inonu University, Department of Computer Engineering, Malatya, Turkey
[c] Namik Kemal University, Department of Electronics and Communication Engineering, Tekirdag, Turkey

ARTICLE INFO

Article history:
Received 13 June 2021
Revised 15 September 2021
Accepted 1 October 2021
Available online 23 October 2021

Keywords:
Fractional order derivative
Approximate realization
Analog circuit design

ABSTRACT

There is a growing interest in fractional calculus and Fractional Order (FO) system modeling in many fields of science and engineering. Utilization of FO models in real-world applications requires practical realization of FO elements. This study performs an analog circuit realization of approximate FO derivative models based on Modified Stability Boundary Locus (M-SBL) fitting method. This study demonstrates a low-cost and accurate analog circuit implementation of M-SBL fitting based approximate model of FO derivative elements for industrial electronics. For this purpose, a 4th order approximate derivative transfer function model of the M-SBL method is decomposed into the sum of first order low-pass filters form by using Partial Fraction Expansion (PFE) method, and the analog circuit design of the approximate FO derivative model is performed. Firstly, by using the final value theorem, authors theoretically show that the time response of the sum of first order low-pass filter form can converge to the time response of fractional order derivative operators. Then, the approximation performance of proposed FO derivative circuit design is validated for various input waveforms such as sinusoidal, square and sawtooth waveforms via Multisim simulations. Results indicate an accurate realization of the FO derivative in time response (an RMSE of 0.0241). The derivative circuit realization of the M-SBL fitting model in the form of the sum of first order low pass filters can yield a better time response approximation performance compared to the Continued Fraction Expansion (CFE) based ladder network realization of the approximate derivative circuit.

1. Introduction

Fractional calculus allows more realistic representation of real-world phenomena. Therefore, FO operator has been widely utilized in the applied science and engineering problems for modeling purposes, for instance in control systems [1–3], mechanics [4–6], energy [7], material modeling [8,9], battery and capacitance [10–12], chaos [13–15]. Although operators of fractional calculus provide more accurate modeling of real-world dynamics in comparison with integer order counterparts, the implementation of the FO derivative and integral operators is not as straightforward as the implementation of integer order derivative and integral operators. A major complication in realization of the FO elements originates from the fact that FO operators perform non-local operation and introduce a long-term, backward memory effect that considers all past values of a function while processing the current value of the derivative of the function. As processing long-term data, this property causes continuously growing computational complexity when implementing a near-ideal FO element in the digital systems [16]. Even for the non-ideal experimental realization of fractional elements, real-time computation efforts may need a faster digital hardware such as the field programmable gate array (FPGA) [15,17,18].

A practical and low-cost solution that copes with these digital implementation problems came from realization options in the form of analog circuits or engineered materials [16]. This point became a central motivation for the analog realization of the FO elements. Thus, a mixed-mode analog and digital design may deal with digital realization complications of near-ideal FO models and allows practical implementation of these models in daily life applications [16,19]. Numerous works have addressed the analog realization of FO elements and systems: These studies have been

* Corresponding author.
E-mail addresses: murat.koseoglu@inonu.edu.tr (M. Koseoglu), furkan.deniz@inonu.edu.tr (F.N. Deniz), baykant.alagoz@inonu.edu.tr (B.B. Alagoz), halisoy@nku.edu.tr (H. Alisoy).

Peer review under responsibility of Karabuk University.

https://doi.org/10.1016/j.jestch.2021.10.001
2215-0986/

mainly focused on the realization of the integer order approximate transfer function models of the FO derivative or integral operators. This methodology can be categorically referred to as indirect realization methods because it has two stages: The first stage requires obtaining an approximate model of the ideal FO elements by using an integer order approximation method. In the second stage, the approximate integer order model of the FO element is realized by using an analog or digital design methodology. Direct realization methods were applied by using engineered structures and materials that directly yield desired FO responses [8,9,16,20–22]. Carbon black nanostructured dielectrics were shown to have a wideband FO frequency response, and this effect has been utilized for the realization of carbon black based FO capacitor elements [21].

Analog realization studies of FO elements also known as fractance devices [23] can be surveyed shortly in two folds: (i) The works aiming discrete analog realization by using basic passive (e.g., resistors, capacitors) and active (e.g., op-amp, OTA) elements [23–38]. (ii) The works aiming Integrated Circuit (IC) realization of FO elements [16,39–43]. The IC technology can provide higher quality FO element realizations at the lower cost in case of mass production. The discrete analog realization efforts were widely implemented as ladder forms and Foster forms (based on PFE) in the circuit design [19,34,37]. In analog design, CFE and PFE techniques are commonly used to decompose the approximate models into elementary function forms and implement them in the ladder and Foster forms. The analog realization approaches, which benefit from PFE method [19,25,29,34,36–38,44], have been studied for the implementation of FO elements, and this analog design scheme can indeed facilitate the analog realization of integer order transfer function of several approximation methods. The main reason is that a continuous-time analog signal can be expressed as the sum of filter functions with a finite number of poles and zeros [36]. The decomposition of a transfer function to partial fraction terms is quite suitable for analog realization of the approximate transfer functions of derivative elements. A comprehensive survey of the analog realization methods, which are based on voltage and current filter forms, and their applications have been elaborated [19]. Recently, realization simplicity and performance improvements by using PFE method have been reported [29,38,45]. These results became a major motivation of the current study, and authors initially aim to establish a theoretical background that validates applicability of the suggested PFE form for FO derivative realization. This theoretical work is a necessity to present a general analog design framework for the dependable realization of all derivative elements. To this end, authors theoretically demonstrate suitability of the suggested partial fraction decomposition form to converge FO derivative operators. After this theoretical validation, approximate transfer function models of FO derivative elements are decomposed into a sum of first order system models in parallel by employing the suggested PFE form. Thus, each partial fraction can be easily implemented by using the low-pass filter circuits and combined by using a summing amplifier circuit to obtain an analog derivate circuit.

The M-SBL fitting method is one of the contemporary integer order approximation methods, which has been particularly proposed for its implications in control system applications. The M-SBL fitting method is proposed for further enhancement of the stability preservation property of the approximate integer order models. Therefore, M-SBL fitting method essentially considers the matching of stability boundary locus curvatures of ideal FO transfer functions and their approximate transfer function models in a predefined frequency range [46]. To the best of our knowledge, analog realization of M-SBL fitting method has not been studied adequately. The current study illustrates an analog realization of the approximate FO derivative functions that are produced by using M-SBL fitting method. Accordingly, the approximate model of the 4th order M-SBL fitting method is decomposed into the sum of partial fraction terms, and each partial fraction is implemented by a first order low-pass active filter that is realized by using an LF347N opamp, two resistors and a capacitor. The implementation results are compared with the results obtained by analog circuit realization of the fractance device based on 5th order rational CFE approximation of $s^{0.5}$ presented in [31]. The current study is devoted to design and validation stages of the approximate FO derivative circuits that are based on the M-SBL fitting method.

The main contributions of the study can be briefly explained as follows:

* This study is the first demonstration for an analog circuit realization of the M-SBL fitting based approximate FO derivative operators. The circuit configuration, which was designed suitable for FO integral operators in the form of the sum of low-pass filters [38], was modified to perform the approximate realization of FO derivative elements, and the proposed analog circuit design is used to implement M-SBL fitting based approximate FO derivative operators.

* Multisim simulation results validate the circuit design for functional tests that were conducted for unit step, sinusoidal, square and sawtooth input waveforms. Bode diagrams are presented to validate operational performance of the circuit design. Results indicate high consistency between results of the theoretical M-SBL model and its analog circuit realization with the low-cost electronic components. This advantage is an important step towards the industrialization of FO elements [16]. Monte Carlo analysis was carried out in the Multisim simulation environment, and the effects of standard component tolerances on the circuit performance are discussed.

* RMSE rates of unit step responses of 4th order models for CFE, Matsuda and M-SBL approximation methods were compared for the derivative $s^{0.5}$ in the frequency range of $\omega \in [0.01, 100]$. It is firstly reported that the M-SBL fitting method can provide better RMSE rates compared to CFE and Matsuda methods for implementation of the $s^{0.5}$. Selection of the approximation method with the lowest RMSE rate is important for the circuit realization.

* A comparative study to evaluate the analog realization performance is conducted with 5th order derivative model of CFE method, which was mentioned to perform better than the Oustaloup method in a former study [31]. It was observed that the 4th order derivative model of the M-SBL method for the derivative $s^{0.5}$ can provide a better realization performance even though its model order is relatively lower.

* An effective analog circuit design form, which is the sum of 1st order low pass filters, is investigated for PFE based realization of FO derivative elements. Simulation results indicate that this realization form is relatively more accurate and presents more design flexibility compared to the ladder network based fractance realization of the CFE method [31]. These properties can be advantageous for the industrial use of FO elements.

2. Theoretical background

2.1. A brief survey of modified SBL method

The approximation methods allow low-complexity and practical realization of FO elements that can operate in a limited operating range of applications, and these methods have played a substantial role in the development of FO control practice by enabling the simulation and implementation of the FO models in control systems. Some fundamental approximation methods, which have been utilized in FO control applications, are Oustaloup's method [47,48], CFE method [47,49], Matsuda's method

[47,50]. From the control applications point of view, the preservation of stability states between the approximate model and the actual models is an important property. Therefore, an approximation method based on the matching stability boundary locus of the approximate and actual models has been proposed, and this approximation method is called the SBL fitting method due to the enabling a better fitting between SBL curves of the approximate and actual models in a desired frequency range [51,52]. The SBL fitting method can be used for the approximate modelling of the FO transfer functions as well as FO integral and derivative elements. Later, a modified version of the SBL fitting method has been suggested as an improvement of SBL fitting to better represent the FO derivative operators [46].

Fig. 1 shows fitting of SBL curves of the fractional order derivative $s^{0.5}$ and the resulting 4th order approximate transfer function of the M-SBL method.

In this figure, overlapping of these SBL curves for all values of PI controller coefficients k_p and k_i allows matching of time, frequency and the stability responses of both models in a given frequency range. Such matching of SBL curves of the FO operator and the approximate models can allow matching of stability states of both models. Thus, it can enhance the stability preservation in the realization of FO elements. This property can be particularly useful for FO controller realization for industrial control applications. Table 1 shows stability states for a series of original FO transfer function models and their M-SBL fitting based approximate models. In the case of slight parametric perturbations of the original function, the matching of stability states indicates the existence of stability preservation property for these systems.

Fig. 2 shows the frequency response matching performances of M-SBL method, Matsuda method and CFE method. The magnitude and phase matching performances of the M-SBL method are comparable with the other approximation methods (See Appendix B for a Matlab code of SBL fitting method). It is also useful to consider the frequency response approximation performances of these methods when the order α values are very close to integer orders $\{1,0,-1\}$. These methods can also be used for the approximate implementation of almost-PID controllers that have fractional order very close to 1 and -1. (See Appendix C to compare approximation performances of the methods for FOs close to 1 and -1.)

A disadvantage of the M-SBL method is that the lower boundary of the frequency range should be set close to zero rad/sec frequency. For this reason, the M-SBL method is not effective when the lower boundary of frequency range is shifted toward higher frequencies.

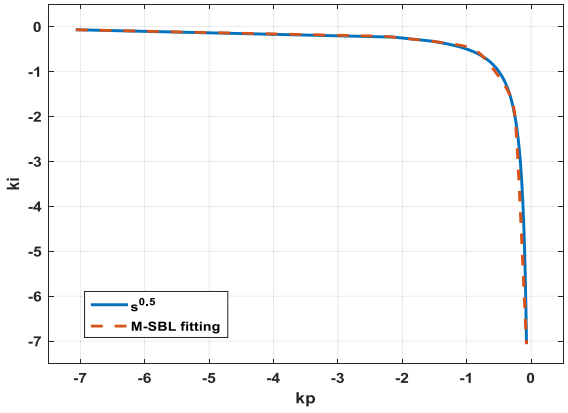

Fig. 1. SBL curves of the FO derivative $s^{0.5}$ and the 4th order approximate model of the M-SBL fitting method in the frequency range of $\omega \in [0.01, 100]$.

Table 1
Stability states of the perturbed fractional order transfer function models and their approximate models with M-SBL fitting method for $\omega \in [0.01, 10]$.

Perturbed FO Transfer Function	Original Transfer Functions	Approximate Transfer Function with M-SBL Method
$T_{f1}(s) = \frac{1}{s^{0.8}-1.2s^{0.6}+1}$	Stable	Stable
$T_{f1}(s) = \frac{1}{s^{0.8}-1.4s^{0.6}+1}$	Stable	Stable
$T_{f1}(s) = \frac{1}{s^{0.8}-1.6s^{0.6}+1}$	Unstable	Unstable
$T_{f1}(s) = \frac{1}{s^{0.8}-1.8s^{0.6}+1}$	Unstable	Unstable

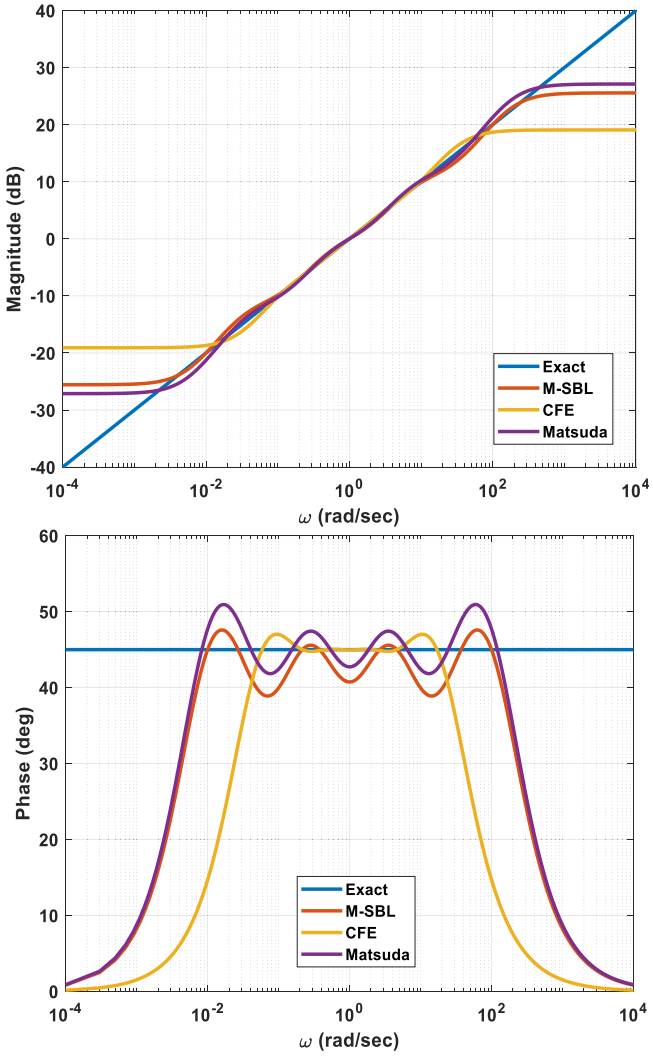

Fig. 2. Bode plots of the 4th order approximate models produced by using M-SBL fitting method, Matsuda method and CFE method for the derivative element $s^{0.5}$ in the frequency range of $\omega \in [0.01, 100]$.

2.2. A general framework for fractional order approximate model realization according to partial fraction decomposition technique

In the system theory, an s-domain model of the FO derivative operation $y(t) = D^{\alpha}f(t)$ is commonly written by the equation $Y(s) = s^{\alpha}F(s)$ by using the Laplace transform, and the FO elements are generally represented by means of dynamic system model of the derivative operators, and they are expressed in the form of a transfer function as [53]

$$T_f(s) = \frac{Y(s)}{F(s)} = s^{\alpha}, \tag{1}$$

where the real number $\alpha \in R$ represents the FO of the derivative operator. (All initial conditions were assumed to be zero in Laplace transform) One can obtain α order derivative of a given $f(t)$ function by observing the dynamic system response of $T_f(s)$ function for the input signal $f(t)$. Thus, it is possible to implement FO derivative operators by synthesizing suitable dynamic system models and realizing them in the hardware forms. Fig. 3 shows a dynamic system-based depiction of FO operators. For $\alpha > 0$, the system $T_f(s)$ performs a FO derivative operation, and for $\alpha < 0$, the system performs a FO integral operation. In the case of $\alpha = 0$, it results in $T_f(s) = 1$, and this case does not perform any operation on the input signal $f(t)$.

A low-complexity approximate implementation of the transfer function s^α has been implemented by using n-th order integer-order approximation functions in the rational form as [16],

$$s^\alpha \cong \frac{a_n s^n + a_{n-1}s^{n-1} + a_{n-2}s^{n-2} + ... + a_2 s^2 + a_1 s + a_0}{b_n s^n + b_{n-1}s^{n-1} + b_{n-2}s^{n-2} + ... + b_2 s^2 + b_1 s + b_0} \tag{2}$$

where the design coefficients are the numerator polynomial coefficients $A = [a_n\ a_{n-1}\ a_{n-2}...a_2\ a_1\ a_0]$ and the denominator polynomial coefficients $B = [b_n\ b_{n-1}\ b_{n-2}...b_2\ b_1\ b_0]$. Optimal approximate integer order transfer function models of s^α are widely based on the limited bandwidth frequency domain approximation techniques, which commonly aim a possible solution of the following generalized optimization problem by using several techniques (e.g., series expansion methods, pole and zero placement methods, curve fitting methods).

$$min\left\{\left| s^\alpha - \frac{a_n s^n + a_{n-1}s^{n-1} + a_{n-2}s^{n-2} + ... + a_2 s^2 + a_1 s + a_0}{b_n s^n + b_{n-1}s^{n-1} + b_{n-2}s^{n-2} + ... + b_2 s^2 + b_1 s + b_0}\right|_{s=j\omega}\right\} \tag{3}$$

Some fundamental approximation methods such as Oustaloup's method, the CFE method, Matsuda's method and the M-SBL fitting method have been surveyed and compared in [46]. After obtaining a satisfactory integer order transfer function approximation of FO derivatives in the form of

$$T_m(s) = \frac{a_n s^n + a_{n-1}s^{n-1} + a_{n-2}s^{n-2} + ... + a_2 s^2 + a_1 s + a_0}{b_n s^n + b_{n-1}s^{n-1} + b_{n-2}s^{n-2} + ... + b_2 s^2 + b_1 s + b_0}, \tag{4}$$

the next step involves implementation of this transfer function in the software or hardware forms. Analog realizations of Oustaloup's method and CFE method have been elaborated in [30]. In the current study, authors utilize the partial fraction decomposition approach for the analog realization of those FO derivative approximation methods. Therefore, the PFE of $T_m(s)$ function is expressed in the following general form:

$$T_m(s) = \frac{r_1}{s-p_1} + \frac{r_2}{s-p_2} + \frac{r_3}{s-p_3} + .. + \frac{r_{n-1}}{s-p_{n-1}} + \frac{r_n}{s-p_n} + k, \tag{5}$$

where the residues are written by the vector $R = [r_n\ r_{n-1}\ r_{n-2}...r_2\ r_1]$, the poles are written by the vector $P = [p_n\ p_{n-1}\ p_{n-2}...p_2\ p_1]$ and the parameter $k \in R$ represents a direct gain [38,44]. In recent works, there is a renewed interest in the partial fraction decomposition form for analog circuit realization of FO elements. This form of partial fraction decomposition has been utilized for passive circuit realization, which was obtained to implement a FO integral operator according to the CFE method [29]. The first and second order filter realizations of different transfer functions by using PFE method have been discussed by considering current and voltage mode circuits [44]. A notable property of $T_m(s)$ function is that the PFE in the form of Eq. (5) reduces the steady state approximation error while converging to the time responses of the ideal FO derivative elements. This important property theoretically demonstrates the capability of the decomposition form to achieve the convergence of time responses of the approximate model to the time response of the ideal fractional derivative operators even for very long-term computations. One can easily prove this convergence of the $T_m(s)$ function form by using the final value theorem (See Appendix A for the proof of this property).

Practically, each partial fraction term $r_i/(s-p_i)$ can be implemented by using a low-pass filter [38], and the direct gain term k can be implemented by the wide-band operational amplifiers. To realize the transfer function, the sum of the partial fraction terms $r_i/(s-p_i)$ and the gain term k can be realized by using the summing amplifier circuits [38]. The function $T_m(s)$ for the n^{th} order approximate realization of the derivative elements can be expressed in more compact form as [44]

$$T_m(s) = k + \sum_{i=1}^{n} \frac{r_i}{s-p_i}. \tag{6}$$

A general block diagram of this partial fraction decomposition based analog realization approach is shown for the derivative elements in Fig. 4. A similar version of this circuit architecture for the approximate FO integral realization by using opamp components has been designed by Yuce et al. [38]. A passive circuit realization of this form according to serial connection of RC passive filters has been also considered for the integral operator realization by Krishna [29].

3. Analog design and realization

3.1. Analog design of partial fraction terms

Analog design can be realized in a simplified way, which is similar to the method mentioned in former studies [38,44]. Each first-order partial fraction term $r_i/(s-p_i)$ can be implemented by using a low-pass filter that is shown in Fig. 5a.

The transfer function of the circuit in Fig. 5a is written as [38]

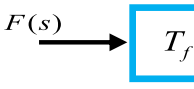

Fig. 3. Transfer function modeling of the fractional order operators.

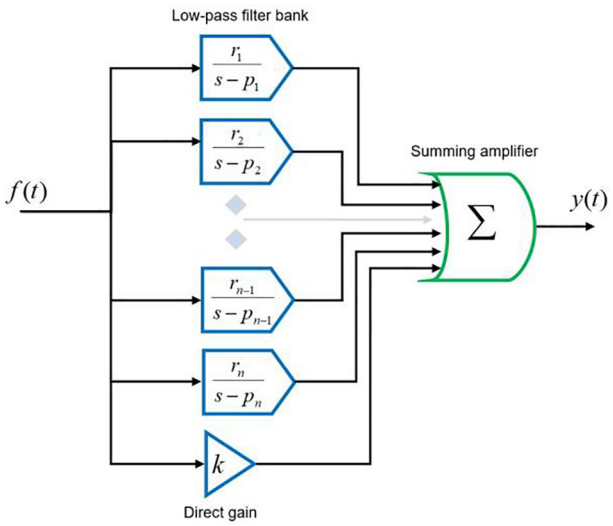

Fig. 4. Transfer function modeling of the fractional order operators.

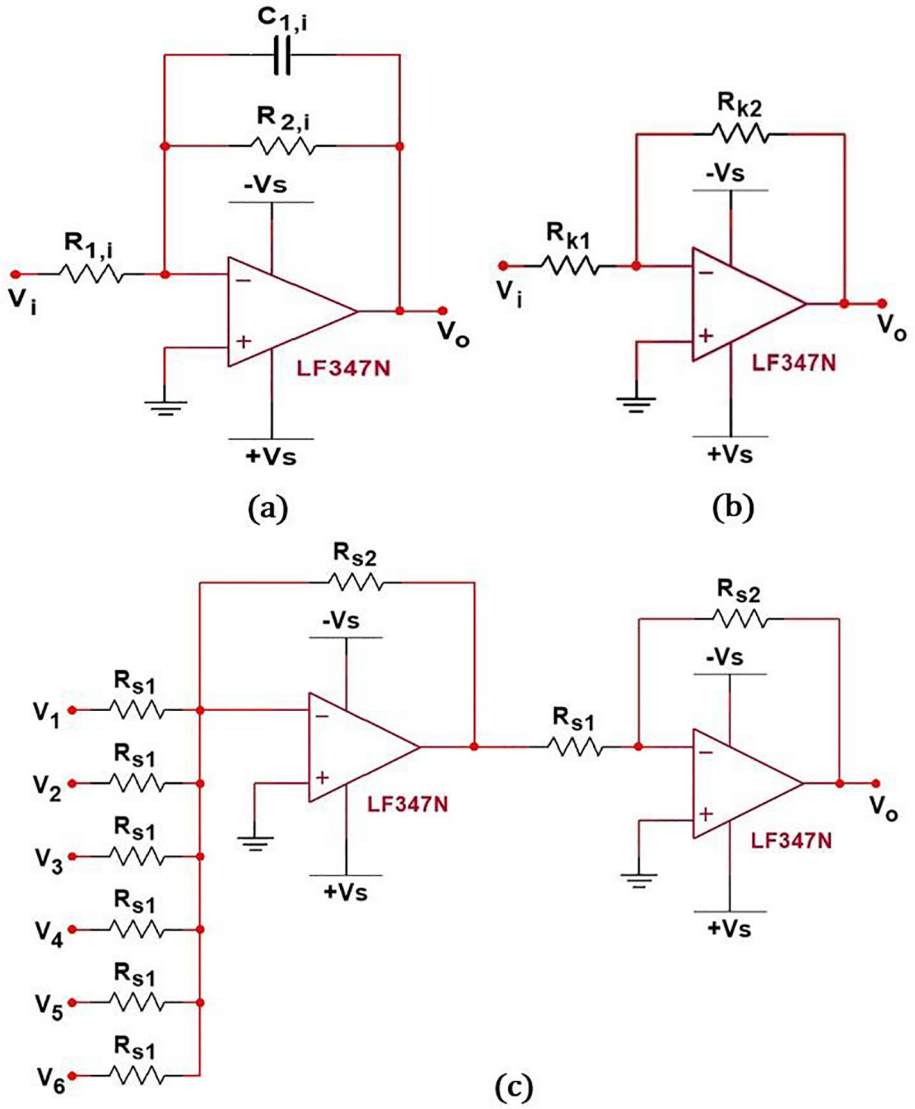

Fig. 5. a) The low-pass filter circuit used to implement first-order partial fraction terms; b) The inverting opamp circuit used to implement a direct gain term; c) The non-inverting analog voltage summing circuit.

$$G_{f,i}(s) = \frac{V_{of,i}}{V_f} = -\frac{1/(R_{1,i}C_{1,i})}{s + \frac{1}{R_{2,i}C_{1,i}}}. \tag{7}$$

To design the low-pass filter circuit and implement the term $r_i/(s-p_i)$, a design rule is widely drawn by equating the transfer functions as

$$-\frac{\frac{1}{R_{1,i}C_{1,i}}}{s + \frac{1}{R_{2,i}C_{1,i}}} = \frac{r_i}{s - p_i} \tag{8}$$

Then, the design rules can be obtained as $r_i R_{1,i} C_{1,i} = -1$ and $p_i R_{2,i} C_{1,i} = -1$ by applying the coefficient matching technique. In the case of an analog realization with discrete components, since a precise configuration of the capacitor components is rather difficult, designers can select a standard capacitor value $C_{1,i} = C_S$ for all filters, then the design rules for discrete analog realization can be written for the determination of resistor values by

$$R_{1,i} = \frac{-1}{C_S r_i} \text{ and } R_{2,i} = \frac{-1}{C_S p_i}. \tag{9}$$

where partial decomposition yields $r_i < 0$ and $p_i < 0$. To implement the direct gain k, an inverting operational amplifier circuit can be used as shown in Fig. 5b. The figure shows a schematic of the inverting operational amplifier. The transfer function of the inverting operational amplifier circuit in Fig. 5b is written by [38]

$$G_k(s) = \frac{V_{ok}}{V_f} = -\frac{R_{k2}}{R_{k1}} \tag{10}$$

To design the gain circuit, which implements the term k in the partial fraction expansion, the transfer function of the amplifier circuit is equated to the term k as follows:

$$-\frac{R_{k2}}{R_{k1}} = k \tag{11}$$

For a convenient resistor value of R_{k1}, the value of R_{k2} can be obtained as

$$R_{k2} = |kR_{k1}| \tag{12}$$

A classical summing amplifier circuit with the voltage inversion can be used to add up all partial fraction terms. To implement the sum block in Fig. 4, an inverting voltage summing amplifier circuit is connected to an inverting amplifier circuit. Fig. 5c shows a sche-

matic diagram of the non-inverting summing amplifier circuit that is used for the analog summing operation of voltages from the circuits that realize partial fraction terms.

By taking $R_{S2} = R_{S1}$, the output of the non-inverting summing amplifier circuit in Fig. 5c is written by [38]

$$V_{out} = V_{of,1} + V_{of,2} + \ldots + V_{of,(n-1)} + V_{of,(n)} + V_{ok} \tag{13}$$

When the entire sub-systems are connected according to the block diagram in Fig. 4, the transfer function of the complete analog circuit ($T_{mr}(s)$), which is the partial fraction decomposition form in Eq. (6), can be expressed as

$$T_{mr}(s) = \frac{V_{out}}{V_f} = \sum_{i=1}^{n} \frac{\frac{1}{R_{1,i}C_{1,i}}}{s + \frac{1}{R_{2,i}C_{1,i}}} + \frac{R_{k2}}{R_{k1}} \tag{14}$$

Fig. 6 shows the analog circuit realization of the approximate FO derivative function by using a wideband JFET input operational amplifier LF347N in the Multisim simulation environment [54]. The LF347N is a low-cost operational amplifier that provides a wider bandwidth and fast slew rates with the low input bias currents. These properties are very useful for real-world applications. In the realization process, 741 opamp was also tested, however, the LF347N was preferred as the active component due to its better step and frequency response.

For a comparative analysis, analog ladder network realization of 5th order rational CFE approximation of $s^{0.5}$ [31] is also implemented in Multisim via two LF347N opamps. Results of circuits are compared in the following section.

3.2. Analog realization examples of approximate fractional order derivative

Example Design: Let us design an analog circuit for 4th order approximate transfer function of the derivative $T_f(s) = s^{0.5}$ according to the M-SBL fitting method to implement the FO derivative operator $D^{0.5}f(t)$.

In realization studies, a demonstration for the order 0.5 has been commonly preferred. Therefore, authors implement $s^{0.5}$ to perform a comparative study and demonstrate consistency of the realization method for FO derivative elements. The M-SBL fitting method yields an approximate transfer function model of the derivative $s^{0.5}$ for a frequency range $\omega \in [0.01, 100]$ rad/sec as

$$T_m(s) = \frac{18.99s^4 + 655.5s^3 + 1301s^2 + 179.7s + 1}{s^4 + 179.7s^3 + 1301s^2 + 655.5s + 18.99} \tag{15}$$

This function is decomposed as

$$T_m(s) = \frac{-2741.4948}{s + 172.2172} + \frac{-15.6015}{s + 6.9900} + \frac{-0.3048}{s + 0.5113} + \frac{-0.0058}{s + 0.0308} + 18.987 \tag{16}$$

where the residues are written by $R = [-2741.4948 \ -15.6015 \ -0.3048 \ -0.0058]$, the poles are written by $P = [-172.2172 \ -6.9900 \ -0.5113 \ -0.0308]$ and the direct gain parameter is $k = 18.987$. Table 2 shows a list of the design parameters for the predefined component values, which are $C_S = 10^{-6}$ F and $R_{k1} = R_{S2} = R_{S1} = 10^3$ Ω.

Fig. 7 shows step responses for the exact analytical solution of the $s^{0.5}$, 4th order approximate models of $s^{0.5}$ according to the M-SBL fitting method, Matsuda method, CFE method, and analog real-

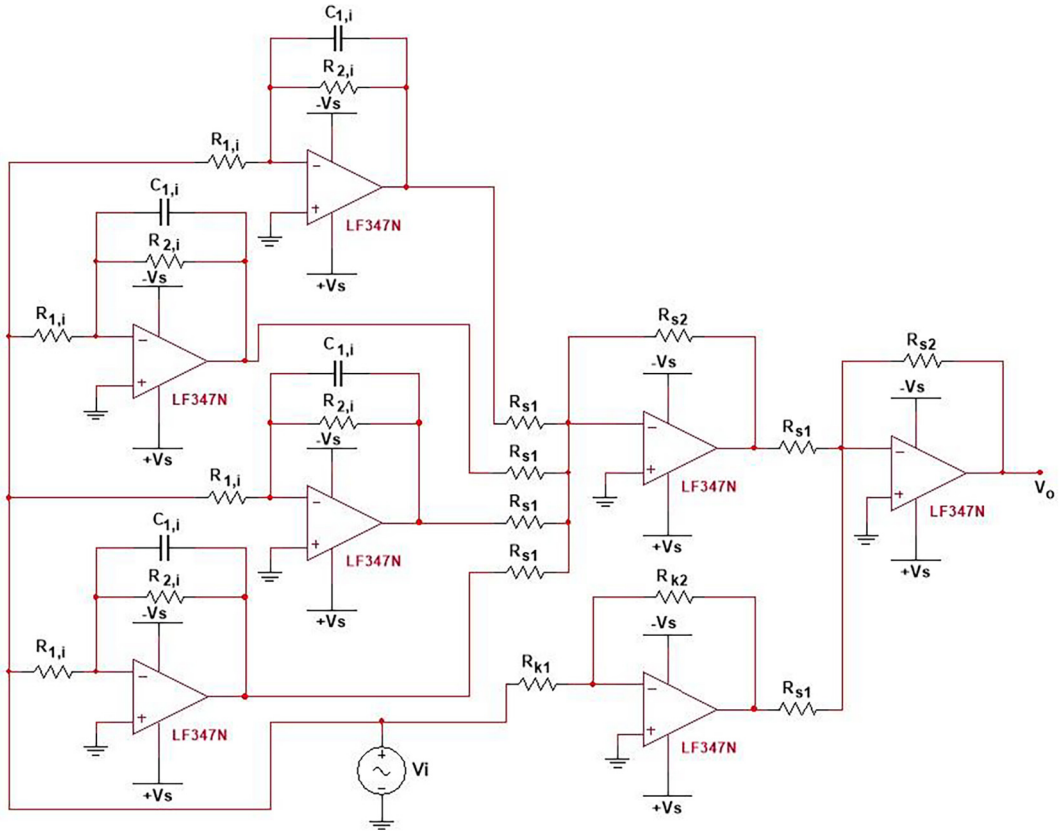

Fig. 6. A schematic of Multisim [54] analog circuit realization of the 4th order approximate FO derivative transfer function according to the partial fraction decomposition technique.

Table 2
The passive component values for 4th order approximate realization of $T_f(s) = s^{0.5}$ according to M-SBL fitting method.

Term Index	Component Values	Partial Fraction Expansion Terms
1	$C_{1,1} = 10^{-6}$F, $R_{1,1} = 364.76\ \Omega$, $R_{2,1} = 5.81 \cdot 10^3 \Omega$	$\frac{-2741.4948}{s+172.2172}$
2	$C_{1,2} = 10^{-6}$F, $R_{1,2} = 6.41 \cdot 10^4 \Omega$, $R_{2,2} = 1.43 \cdot 10^5\ \Omega$	$\frac{-15.6015}{s+6.9900}$
3	$C_{1,3} = 10^{-6}$F, $R_{1,3} = 3.28 \cdot 10^6\ \Omega$, $R_{2,3} = 1.96 \cdot 10^6\ \Omega$	$\frac{-0.3048}{s+0.5113}$
4	$C_{1,4} = 10^{-6}$F, $R_{1,4} = 1.73 \cdot 10^8 \Omega$, $R_{2,4} = 3.24 \cdot 10^7 \Omega$	$\frac{-0.0058}{s+0.0308}$
5	$R_{k1} = 10^3 \Omega$, $R_{k2} = 1.90 \cdot 10^4\ \Omega$	18.9868

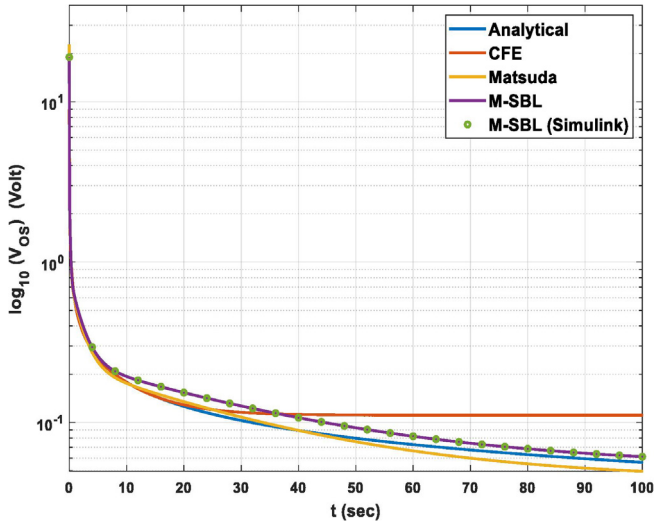

Fig. 7. Step responses for the exact analytical solution of $s^{0.5}$, the 4th order approximate models of M-SBL fitting method, Matsuda method and CFE method and the Simulink analog realization of M-SBL method.

ization of M-SBL method. The simulation results indicate that the lowest RMSE value in step response is observed for the M-SBL fitting method. The RMSE value for M-SBL method is 0.02410, while that is 0.05260 for CFE and 0.03003 for Matsuda's method. These RMSE values were calculated for 100 sec unit step response with a time increment of 0.001 sec. Fig. 7 reveals that step responses of the M-SBL model $T_m(s)$ (Eq. (15)) and M-SBL based analog circuit realization model $T_{mr}(s)$ in Simulink are perfectly overlapping (the RMSE is about $1.48 \cdot 10^{-5}$). A reason for this matching performance is that the Simulink analog circuit simulation models use ideal models of circuit components from the Simscape library [55]. Besides, the figure demonstrates that the Simulink analog circuit realization model $T_{mr}(s)$ can well approximate to the exact analytical solution that is expressed by using inverse Laplace transform of s^{α} as

$$y(t) = L^{-1}\{\frac{1}{s}s^{\alpha}\} = \frac{1}{\Gamma(1-\alpha)}t^{\alpha} \quad (17)$$

Authors also performed the Multisim [54] simulations by using more realistic models of the existing standard electronics components. Multisim simulations of the fractional derivative were carried out according to the values of design parameters in Table 2. Fig. 8 illustrates the simulation results for square and sawtooth input signal waveforms. For these input waveforms, transient responses for Multisim M-SBL based sum of the filter form (Multisim M-Sbl), Simulink M-SBL based sum of the filter form (Simulink M-Sbl), 4th order M-SBL fitting model $T_m(s)$ (M-Sbl) and Multisim CFE based ladder network [31] (Multisim CFE) are presented in figures comparatively. Derivative operators yield sharp peaks at the edges of the input signals. This property is observed in the simulation results in Fig. 8, and it confirms correct functioning of the circuit for the derivative operation. Slight differences in Multisim and Simulink simulation results of M-SBL fitting based circuits are caused by non-ideal characteristic of LF347N opamps, which were supplied with ± 18 V in the simulations. The consistency in responses of theoretical M-SBL fitting model $T_m(s)$ and its Multisim circuit realization indicates effectiveness of the sum of filters form for the analog realization of transfer function. The figure also reveals that the proposed M-SBL based analog circuit realization in the sum of filters form yields more proper derivative responses compared to those of CFE based ladder network [31].

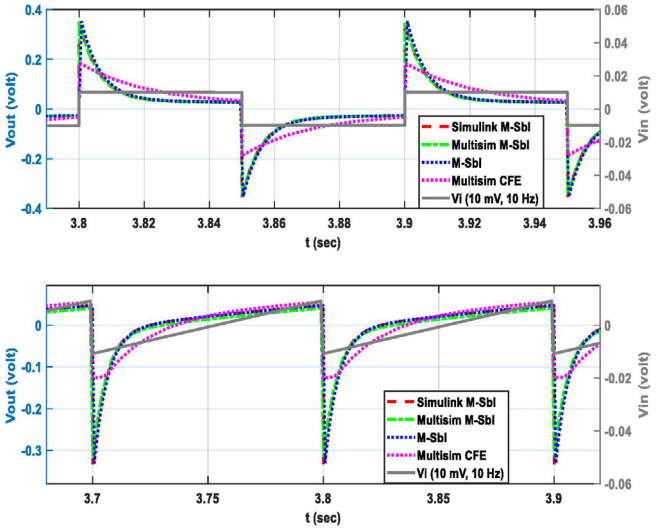

Fig. 8. Square and sawtooth wave responses of the M-SBL based sum of the filter from realization in Multisim (Multisim M-Sbl), the M-SBL based sum of the filter form realization in Simulink (Simulink M-Sbl), the 4th order M-SBL fitting model $T_m(s)$ (M-Sbl) and the 5th order CFE based ladder network [31] (Multisim CFE).

It is also useful to observe responses of the system for sinusoidal input signals in order to evaluate phase and magnitude modifications of the FO derivative operator on the input signal. Thus, one can investigate the relevance of time responses of the circuits for the FO derivative behavior at each frequency component. Sinusoidal waveforms can be expressed in the form of $M_0 sin(\omega t + \theta_o)$, where the angular frequency is $\omega = 2\pi f$, the initial amplitude is M_o and the initial phase is θ_o. An ideal fractional order derivative operator yields $M_0\omega^{\alpha} sin(\omega t + \theta_o + \alpha \cdot \pi/2)$ at the output for this input signal. Hence, a FO derivative operator modifies the amplitude of input sinusoidal component as exactly $M_0\omega^{\alpha}$ and the phase as exactly $(\theta_o + \alpha \cdot \pi/2)$.

Fig. 9 shows simulation results for sinusoidal input signals at $f = 1$ Hz, $f = 10$ Hz and $f = 100$ Hz. The figure validates accurate functioning of the proposed M-SBL based analog circuit realization for the sampled frequencies within an approximation range of $\omega \in [0.01, 100]$ rad/sec. The Multisim and Simulink simulation results of the M-SBL based analog circuit well agree with the theoretical results obtained by using M-SBL fitting method for 4th order approximate transfer function $(T_m(s))$ of $s^{0.5}$. This observation indicates that the analog circuit design is not severely affected by the limitations of realistic component models in the Multisim. When Multisim simulation results of 4th order M-SBL based sum of the filter circuit and 5th order CFE based ladder network are compared for sinusoidal input waveforms in Fig. 9, it is seen that

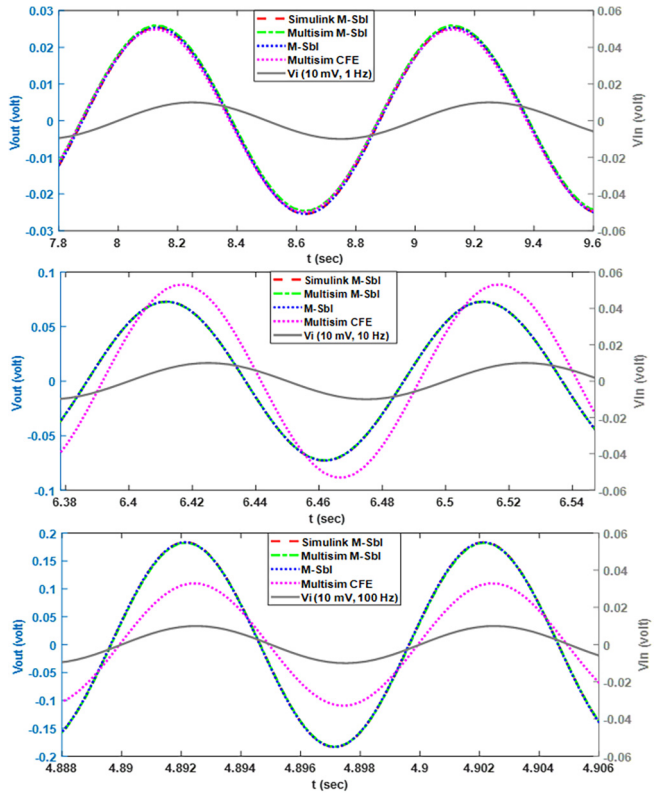

Fig. 9. Comparative sine wave responses of the 4th order M-SBL and 5th order CFE approximate transfer functions for $s^{0.5}$ at different frequencies.

the results agree with each other at 1 Hz, while they differ considerably at 10 Hz and 100 Hz. The amplitude and phase values of the output signal from the CFE based ladder circuit diverge from the expected values at these frequencies. These findings indicate that the CFE based realization circuit cannot well operate at higher frequencies (The approximation frequency range is not configurable in the CFE method).

Table 3 lists the phase and amplitude modification results for the analytical calculation, the proposed M-SBL based sum of the filters form realization and the CFE based ladder network realization in Multisim, and the consistency of amplitude and phase modifications with the analytical calculation up to 100 rad/sec validates that the proposed M-SBL based analog circuit provides a satisfactory approximation performance to perform FO derivative $s^{0.5}$ in the frequency range of $\omega \in [0.01, 100]$ rad/sec. Especially, for the frequency values of 50 rad/sec and greater, phase responses of the CFE based derivative circuit diverge from exact values compared to the response of the M-SBL based circuit. Since $\omega = 200$ rad/sec and $\omega = 500$ rad/sec are out of the frequency range $\omega \in [0.01, 100]$ rad/sec, the approximation performance of M-SBL method begins to decrease at $\omega = 200$ rad/sec and $\omega = 500$ rad/sec frequencies in Table 3. To improve magnitude and phase approximation performances at these frequencies, the frequency range configuration of the SBL fitting method can be increased to include these frequencies.

To compare realization performances of analog circuit designs in the Multisim simulation environment, authors analysed the time and frequency response matching performances of two analog circuit designs. Fig. 10 shows Bode diagrams for the exact model ($s^{0.5}$), theoretical 4th order M-SBL transfer function ($T_m(s)$), the 4th order M-SBL fitting based analog circuit realization in the sum of filters form and the 5th order CFE based circuit realization in the ladder network form [31]. One can validate effective operating ranges of the designed analog realization circuits in Bode diagrams. Fig. 10 confirms that the M-SBL fitting based analog circuit can perform as an approximate FO derivative operator within the specified frequency range of $\omega \in [0.01, 100]$. These Bode diagrams indicate that the frequency response of the M-SBL fitting based analog circuit realization in Multisim diverges from the calculated frequency response of the transfer function ($T_m(s)$) of the M-SBL fitting method at very low frequency values. This effect is mainly caused by the limitations and non-ideal characteristics of the LF347N components in the Multisim, where operational amplifier models introduce the realistic bandwidth limitations and the finite input resistance. These limitations of realistic models in Multisim result in early divergence of the frequency responses of the M-SBL fitting based derivative circuit from those of the M-SBL transfer function model at very low frequencies. However, this divergence seen in the frequency responses emerges at the out of the operating frequency range $\omega \in [0.01, 100]$ rad/sec. Inside the operating frequency range, the frequency responses of the transfer function model and its Multisim circuit realization are very consistent with each other. The RMSE performances of two analog circuit realizations are also reported in Table 4. One observes that the proposed 4th order M-SBL based analog derivative circuit realization can demonstrate much better time response and phase response matching performances than those of the 5th order CFE based approximate derivative circuit. However, the magnitude response matching performance of 4th order M-SBL based approximate derivative circuit is at a comparable level with the 5th order CFE based approximate derivative circuit.

3.3. Monte Carlo analysis

Monte Carlo simulation of the proposed M-SBL fitting based derivative circuit was conducted for 5% tolerance of each component value according to the Gaussian distribution. (The standard carbon film resistors have 5% tolerance) Monte Carlo simulations were performed for 2000 trials in the Multisim simulation environment. The input of the derivative circuit was a sinusoidal waveform with 10 mV amplitude and 10 Hz frequency. Fig. 11 shows the circuit outputs from the Monte Carlo simulation. Results indi-

Table 3
The amplitude and phase modifications for the derivative operator $s^{0.5}$ that are obtained by analytical calculations $\{M_0\omega^{\alpha}, (\theta_o + \alpha \cdot \pi/2)\}$ and the analog realizations ($T_{mr}(s)$) of the 4th order approximate M-SBL based circuit and 5th order approximate CFE based circuit.

Angular Frequency $\omega = 2\pi f$(rad/sec)	Analytical (Exact) Amp. (dB)	Phase (deg)	M-SBL Multisim Simulation Amp. (dB)	Phase (deg)	CFE Multisim Simulation Amp. (dB)	Phase (deg)
1 (0.159 Hz)	0	45	−0.00106	40.7445	0.03314	45.3775
5 (0.796 Hz)	6.9897	45	7.0333	44.6477	6.9755	44.8582
10 (1.592 Hz)	10	45	9.8664	39.9554	9.9472	45.9590
50 (7.96 Hz)	16.9897	45	15.9208	47.0153	18.1653	34.6614
100 (15.92 Hz)	20	45	19.9971	44.9907	19.9823	20.9292
200 (31.84 Hz)	23.0103	45	23.2658	33.0583	20.6141	10.8864
500 (79.58 Hz)	26.9897	45	25.0968	15.8844	20.8103	3.7080

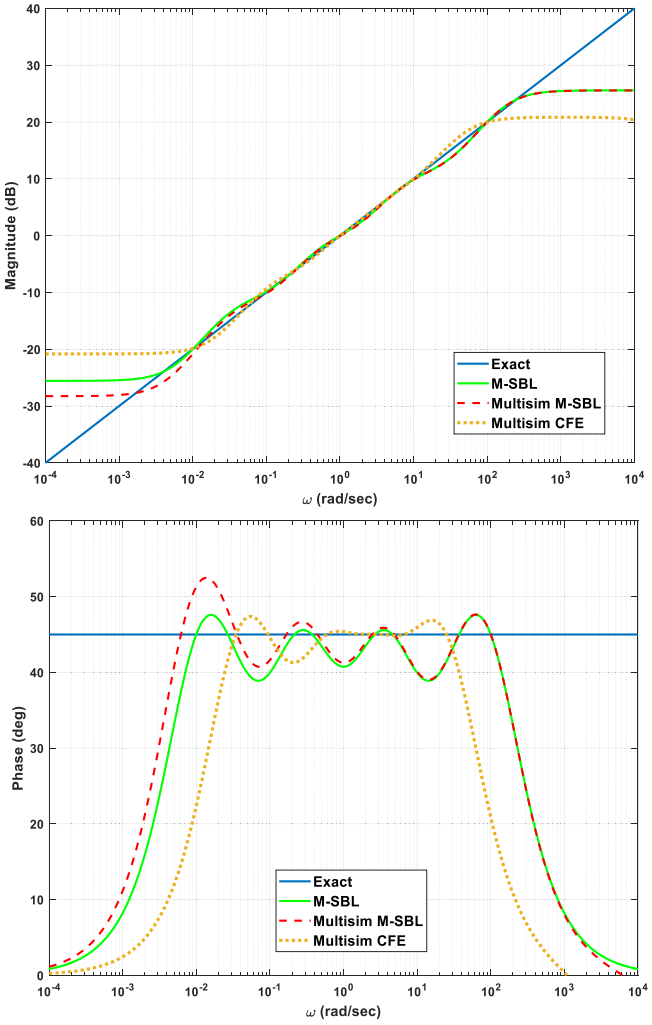

Fig. 10. Bode diagrams for the exact analytical solution of $s^{0.5}$, the 4th order approximate model by M-SBL fitting method, and the 5th order approximate model by CFE method.

Table 4
Time and frequency domain RMSE performances of the M-SBL fitting based derivative circuit in sum of low-pass filter form and the CFE based realization in the ladder network form.

Realization Approaches	RMSEs in step response (100 sec)	RMSEs in magnitude response	RMSEs in phase response
4th order M-SBL based realization in the form of the sum of low-pass filters	0.0241	0.6084206	3.405755
5th order CFE based realization in the ladder network form in Ref [31]	0.0526	0.5166340	7.171742

cate that the phase and amplitude deformations in output waveforms due to the component tolerance are limited (The output voltage mean value is 0.072 V and the standard deviation in output voltage is obtained 0.0045.) and the circuit can perform the FO derivative function.

Fig. 12 shows the histogram of output voltages from these Monte Carlo simulations. Fig. 13 shows the Bode plots of the proposed circuit for 2000 trials of the Monte Carlo simulation. Results in the figure reveal that sensitivity of frequency response charac-

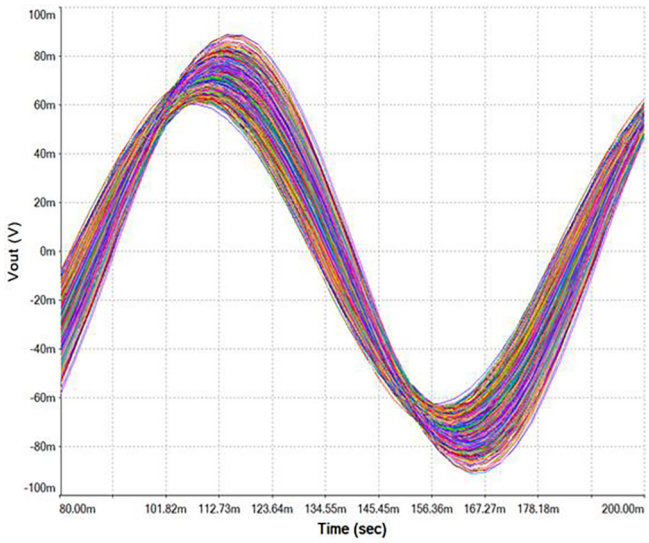

Fig. 11. Monte Carlo simulation results for time response of the proposed M-SBL fitting based derivative circuit in Multisim environment.

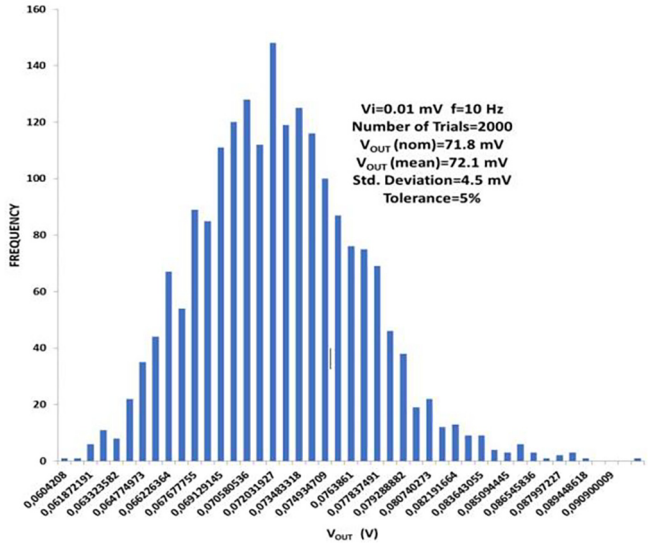

Fig. 12. Histogram from Monte Carlo simulations in Multisim environment for the proposed M-SBL fitting based derivative circuit.

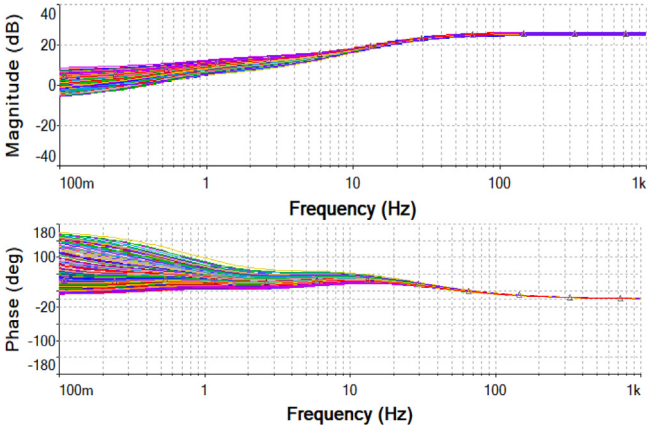

Fig. 13. Multisim Monte Carlo simulation for frequency responses of the proposed M-SBL fitting based derivative circuit.

teristics to the component tolerance decreases toward the higher frequencies.

Parameter sweep analyses of the Multisim simulation indicated that the sensitivity of the circuit output to resistor tolerances of the output amplifiers is high. However, when the low-pass active filters, which are connected to the circuit input, are considered, authors observed that sensitivity of the output to resistor tolerance values is the highest at the first low-pass filter (The partial fraction term index is 1 in Table 2). Filter's cut-off frequencies are 27.41 Hz for the first filter, 1.14 Hz for the second filter, 0.080 Hz for the third filter and 0.049 Hz for the fourth filter. Due to the highest bandwidth of the first filter compared to others, resistor tolerances can alter more the bandwidth of the first low pass filter, and thus more affect the overall gain of the circuit at the output. Therefore, the circuit output is more sensitive to the resistor tolerance of the first low-pass filter compared to other low-pass filters.

4. Conclusions

This study firstly demonstrated the analog circuit realization of M-SBL fitting based approximate FO derivative models according to the sum of low-pass filter form. Another contribution of the study is that comprehensive performance analyses of the proposed analog circuit realization were carried out to verify the factional order behavior of the circuit in both time and frequency domains: Firstly, by using the final value theorem, authors theoretically prove that time responses of the sum of low-pass filter form realization can converge to the time response of any fractional order derivative function (s^{α}). It is useful to demonstrate theoretical limits of the sum of low-pass filter form in convergence to the time response of the FO derivative function s^{α}. Afterward, time responses of the proposed analog derivative circuit were validated for various input waveforms (e.g. sinusoidal, square and sawtooth waveforms) by using two different circuit simulation environments that are the Matlab Simulink simulation model with Simscape library and the Multisim circuit simulator. Frequency response approximation performance was also shown by using Bode diagrams that are drawn according to simulation results. Some important remarks can be summarized as follows:

* Time domain responses of M-SBL fitting based analog circuit realization models are very consistent with time responses of the M-SBL fitting based transfer function model of FO derivative elements. These results indicate that the sum of low-pass filter form realization according to the partial fraction decomposition is an effective and straightforward solution for analog circuit realization problems of transfer function models.

* The step responses of 4th order approximate derivative models of Matsuda, CFE and M-SBL fitting methods are compared according to 100 sec simulation results, and the smallest RMSE value with respect to step response of the derivative $s^{0.5}$ was obtained by using the M-SBL fitting method.

* Two different analog circuit realization approaches are implemented in the Multisim simulation and their approximation performances are compared. These approaches are the sum of the low-pass filters form realization of M-SBL derivative model and the CFE based active realization of FO derivative in the ladder network form [31]. According to Multisim simulation results, it was observed that although the model order of M-SBL based realization was lower than that of the CFE based active realization, the analog realization of the M-SBL based approximate derivative model provided a better approximation performance in comparison to the CFE based ladder network realization in a frequency range of [0.01,100] rad/sec. This performance improvement in analog realization mainly originates from using an active low-pass filter for each partial fraction term of the transfer function model. In the CFE based ladder network realization form, a passive element network in ladder from is used to implement the fractance device.

* Authors concluded that the PFE method in sum of filters form [38,44] is very practical for the analog realization of rational transfer functions because each partial fraction term can be realized independently. The component values of each active filter can be adjusted independently and the selection of component values in a low-pass filter does not affect the rest of the analog circuit unless the filter transfer function changes. This property provides significant design flexibility. For this reason, passive component values can be adjusted more realistic, and they can be easily chosen from the standard and available electronic components. This design flexibility makes the circuit realization more accurate compared to the passive ladder network realization based on the CFE method [31]. The design flexibility and applicability of standard components in realization works of FO elements have not been extensively discussed in the literature [56]. However, design flexibility and realization accuracy are indispensable for the industrial use of FO elements [16].

* Authors observed that the selection of active and passive components can affect both time and frequency response performances of the FO derivative circuits. Therefore, design flexibility of the sum of low-pass filter form realization in component selection is particularly beneficial for improving analog circuit realization performance of the fractional order derivative elements. It is recommended to consider not only frequency response but also step responses of the analog circuit when selecting active components.

* In this study, a low-cost active component, LF347N, was selected after testing several commercial opamp IC options. Multisim simulation results indicated that the use of LF347N opamp in low-pass filters and the sum circuit provided a satisfactory design consistency with the theoretical results. The possible applications of such analog FO derivative circuits can be industrial process control systems. Future works can address the control of industrial processes by using the analog FO derivative circuit. The circuit output shows more sensitivity to component tolerances at very low frequencies. Also, future studies can focus on this issue by improving circuit design for the sum of filters form.

Declaration of Competing Interest

The authors declare that they have no known competing financial interests or personal relationships that could have appeared to influence the work reported in this paper.

Appendix A

Property 1. A long-term time responses of the $T_m(s)$ function with non-zero poles ($p_i \neq 0$) ($T_m(s) = \sum_{i=1}^{n} \frac{r_i}{s-p_i} + k$) can converge to the time response of $T_f(s) = s^{\alpha}$.

Proof. The steady state error between $T_m(s)$ and dynamic model of the derivative operator $T_f(s) = s^{\alpha}$ can be expressed as $e_s(s) = T_f(s) - T_m(s)$. When the steady stead error goes to the zero in time, this ensures the convergence of time responses of both models. For convergence of the steady state to zero in time, the following condition should be satisfied:

$lim_{t\to\infty} e_s(t) = 0$

This condition ensures the convergence of time responses of the models. By using the final value theorem, one can write $lim_{t\to\infty} e_s(t) = lim_{s\to 0^+} s e_s(s)$ and for the approximation of the steady state to zero, the following condition should be satisfied:

$lim_{s\to 0^+} s e_s(s) = 0$

Let us check if this condition is satisfied. When the $e_s(s) = T_f(s) - T_m(s)$ is used in this condition,

$$lim_{t\to\infty} e_s(t) = lim_{s\to 0^+} s e_s(s) = lim_{s\to 0^+} s(T_f(s) - T_m(s))$$

$$lim_{t\to\infty} e_s(t) = lim_{s\to 0^+} s(s^{\alpha} - \frac{r_1}{s-p_1} - \frac{r_2}{s-p_2} - \frac{r_3}{s-p_3} - .. - \frac{r_{n-1}}{s-p_{n-1}} - \frac{r_n}{s-p_n} - k)$$

$$lim_{t\to\infty} e_s(t) = lim_{s\to 0^+} (s^{\alpha+1} - \frac{r_1 s}{s-p_1} - \frac{r_2 s}{s-p_2} - \frac{r_3 s}{s-p_3} - .. - \frac{r_{n-1} s}{s-p_{n-1}} - \frac{r_n s}{s-p_n} - ks)$$

$$lim_{t\to\infty} e_s(t) = lim_{s\to 0^+} (s^{\alpha+1}) - lim_{s\to 0^+} (\frac{r_1 s}{s-p_1}) - lim_{s\to 0^+} (\frac{r_2 s}{s-p_2}) - lim_{s\to 0^+} (\frac{r_3 s}{s-p_3}) - \cdots$$

$$-lim_{s\to 0^+} (\frac{r_{n-1} s}{s-p_{n-1}}) - lim_{s\to 0^+} (ks)$$

For the derivative element $s^{\alpha+1}$ ($\alpha > 0$), then $lim_{s\to 0^+} (s^{\alpha+1}) = 0$ is always valid. For a $T_m(s)$ function with non-zero poles ($p_i \neq 0$), the results $lim_{s\to 0^+} (\frac{r_i s}{s-p_i}) = 0$. $lim_{s\to 0^+} (ks) = 0$ are always valid. Therefore, one can proof that $lim_{t\to\infty} e_s(t) = 0$ is valid, a $T_m(s)$ function with the non-zero poles can converge to any derivative function s^{α}, $\alpha > 0$ without a steady state error.

This property is important to demonstrate the suitability of the partial fraction decomposition in the form of $T_m(s) = \sum_{i=1}^{n} \frac{r_i}{s-p_i} + k$ for the realization of the derivative operation.

Appendix B

M-SBL fitting approximation method Matlab codes:

```
function [Gapx] = M_SBL(Alpha,n,wl,wh)
% M_SBL(Alpha,n,wl,wh)
%Alpha: fractional order of the derivative operator
%n: degree of integer order approximate model
%wl and wh   Lower and Upper bounds of frequency range
%Logarithmically spacing in frequency range [wl, wh]
if n==1
    w=wh;
else
for i=1:n
    w(i)=wl*(wh/wl)^((i-1)/(n-1));
end
end
for k=1:n
    for r=1:n
A(r,k)=(j*w(k))^r-(j*w(k))^(n-r+2)*(cos(pi/2*Alpha))...
    /(w(k)^Alpha)-(j*w(k))^(n-r+1)*(sin(pi/2*Alpha))...
    /(w(k)^(Alpha-1));
A(r,k)=real(A(r,k))+imag(A(r,k));
B(1,k)=-(j*w(k))^(n+1)+(j*w(k))*(cos(pi/2*Alpha))...
    /(w(k)^Alpha)+(sin(pi/2*Alpha))/(w(k)^(Alpha-1));
 B(1,k)=real(B(1,k))+imag(B(1,k));
    end
end
C=(A^(-1))'*(B');
for i=1:length(C)
num=[C' 1];
den=fliplr(num);
end
Gapx=tf(num,den);
```

Appendix C

Frequency response approximation performances of several methods for α values that are very close to integer orders {1,0,−1}. For $\alpha = 0.999$;

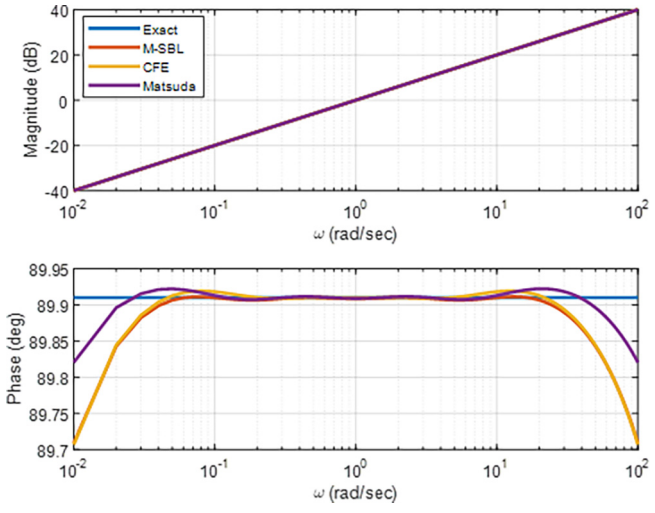

For $\alpha = 0.001$;

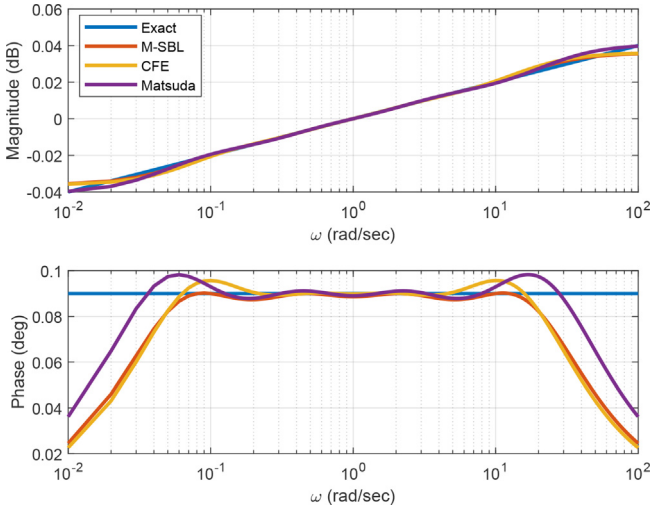

For $\alpha = -0.999$;

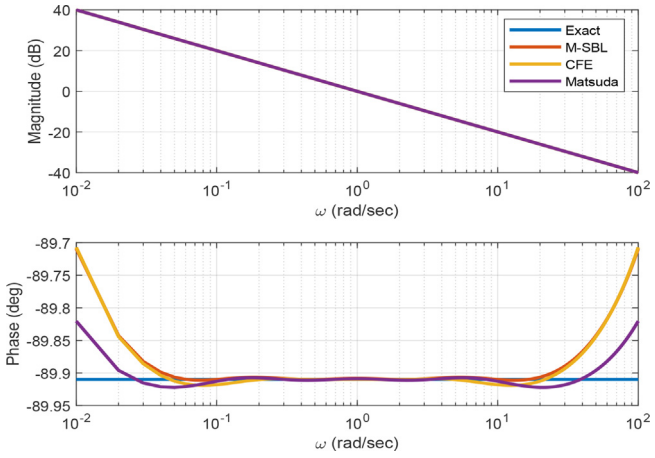

References

[1] R. Caponetto, G. Dongola, L. Fortuna, I. Petráš, Fractional Order Systems: Modeling and Control Applications, World Scientific, Singapore, 2010.

[2] T.T. Hartley, C.F. Lorenzo, Fractional-order system identification based on continuous order-distributions, Signal Process. 83 (11) (2003) 2287–2300, https://doi.org/10.1016/S0165-1684(03)00182-8.

[3] B.B. Alagoz, A. Tepljakov, A. Ates, E. Petlenkov, C. Yeroglu, Time-domain identification of one noninteger order plus time delay models from step response measurements, Int. J. Model. Simul. Sci. Comput. 10 (2019), https://doi.org/10.1142/S1793962319410113.

[4] T.F. Nonnenmacher, W.G. Glöckle, A fractional model for mechanical stress relaxation, Philos. Mag. Lett. 64 (2) (1991) 89–93, https://doi.org/10.1080/09500839108214672.

[5] R.L. Bagley, R.A. Calico, The fractional order state equations for the control of viscoelastically damped structures, J. Guid. Control. Dyn. 14 (1991) 304–311. http://www.elsevier.com/locate/scp.

[6] A. Coronel-Escamilla, J.F. Gómez-Aguilar, L. Torres, R.F. Escobar-Jimnez, V.H. Olivares-Peregrino, Fractional observer to estimate periodical forces, ISA Trans. 82 (2018) 30–41, https://doi.org/10.1016/j.isatra.2017.11.003.

[7] L. Chen, B. Basu, D. McCabe, Fractional order models for system identification of thermal dynamics of buildings, Energy Build. 133 (2016) 381–388, https://doi.org/10.1016/j.enbuild.2016.09.006.

[8] B.B. Alagoz, G. Alisoy, S. Alagoz, H. Alisoy, A note on applications of time-domain solution of Cole permittivity models, Optik (Stuttg). 139 (2017) 272–282, https://doi.org/10.1016/j.ijleo.2017.04.010.

[9] G. Failla, M. Zingales, Advanced materials modelling via fractional calculus: Challenges and perspectives, Philos. Trans. R. Soc. A Math. Phys. Eng. Sci. A378 (2020), https://doi.org/10.1098/rsta.2020.0050.

[10] T.J. Freeborn, B. Maundy, A.S. Elwakil, Fractional-order models of supercapacitors, batteries and fuel cells: A survey, Mater. Renew. Sustain. Energy 4 (2015) 1–7, https://doi.org/10.1007/s40243-015-0052-y.

[11] B.B. Alagoz, H. Alisoy, Estimation of reduced order equivalent circuit model parameters of batteries from noisy current and voltage measurements, Balk. J. Electr. Comput. Eng. 6 (2018) 224–231. 10.17694/bajece.449265.

[12] Y. Wang, T.T. Hartley, C.F. Lorenzo, J.L. Adams, J.E. Carletta, R.J. Veillette, Modeling ultracapacitors as fractional-order systems, in: D. Baleanu, Z.B. Guvenc, J.A.T. Machado (Eds.), New Trends in Nanotechnology and Fractional Calculus Applications, Springer Netherlands, Dordrecht, 2010, pp. 257–262, https://doi.org/10.1007/978-90-481-3293-5_21.

[13] A. Silva-Juárez, E. Tlelo-Cuautle, L.G. de la Fraga, R. Li, FPAA-based implementation of fractional-order chaotic oscillators using first-order active filter blocks, J. Adv. Res. 25 (2020) 77–85, https://doi.org/10.1016/j.jare.2020.05.014.

[14] T.T. Hartley, C.F. Lorenzo, H. Killory Qammer, Chaos in a fractional order Chua's system, IEEE Trans. Circuits Syst. I Fundam. Theory Appl. 42 (8) (1995) 485–490.

[15] L.F. Ávalos-Ruiz, C.J. Zúñiga-Aguilar, J.F. Gómez-Aguilar, R.F. Escobar-Jiménez, H.M. Romero-Ugalde, FPGA implementation and control of chaotic systems involving the variable-order fractional operator with Mittag-Leffler law, Chaos, Solitons and Fractals 115 (2018) 177–189, https://doi.org/10.1016/j.chaos.2018.08.021.

[16] A. Tepljakov, B.B. Alagoz, C. Yeroglu, E.A. Gonzalez, S. Hassan Hosseinnia, E. Petlenkov, A. Ates, M. Cech, Towards industrialization of FOPID controllers: A survey on milestones of fractional-order control and pathways for future developments, IEEE Access 9 (2021) 21016–21042, https://doi.org/10.1109/access.2021.3055117.

[17] K.P.S. Rana, V. Kumar, N. Mittra, N. Pramanik, Implementation of fractional order integrator/differentiator on field programmable gate array, Alexandria Eng. J. 55 (2) (2016) 1765–1773, https://doi.org/10.1016/j.aej.2016.03.030.

[18] C.X. Jiang, J.E. Carletta, T.T. Hartley, R.J. Veillette, A systematic approach for implementing fractional-order operators and systems, IEEE J. Emerg. Sel. Top. Circuits Syst. 3 (3) (2013) 301–312, https://doi.org/10.1109/JETCAS.2013.2272836.

[19] G. Tsirimokou, C. Psychalinos, A. Elwakil, Design of CMOS analog integrated fractional-order circuits, Applications in Medicine and Biology, Springer International Publishing, 2017.

[20] A. Adhikary, M. Khanra, J. Pal, K. Biswas, Realization of fractional order elements, Ina. Lett. 2 (2) (2017) 41–47, https://doi.org/10.1007/s41403-017-0020-1.

[21] K. Biswas, R. Caponetto, G. Di Pasquale, S. Graziani, A. Pollicino, E. Murgano, Realization and characterization of carbon black based fractional order element, Microelectronics J. 82 (2018) 22–28, https://doi.org/10.1016/j.mejo.2018.10.008.

[22] D.A. John, S. Banerjee, G.W. Bohannan, K. Biswas, Solid-state fractional capacitor using MWCNT-epoxy nanocomposite, Appl. Phys. Lett. 110 (2017), https://doi.org/10.1063/1.4981204.

[23] B.T. Krishna, K.V.V.S. Reddy, Active and passive realization of fractance device of order 1/2, Act. Passiv. Electron. Comp. 2008 (2008) 2–7, https://doi.org/10.1155/2008/369421.

[24] G. Carlson, C. Halijak, Approximation of fractional capacitors (1/s)^1/n by a regular newton process, IEEE Trans. Circuit Theory 11 (2) (1964) 210–213, https://doi.org/10.1109/TCT.1964.1082270.

[25] A. Djouambi, A. Charef, A. Besançon, Optimal approximation, simulation and analog realization of the fundamental fractional order transfer function, Int. J. Appl. Math. Comput. Sci. 17 (2007) 455–462, https://doi.org/10.2478/v10006-007-0037-9.

[26] J. Baranowski, M. Pauluk, A. Tutaj, Analog realization of fractional filters: Laguerre approximation approach, AEU - Int. J. Electron. Commun. 81 (2017) 1–11, https://doi.org/10.1016/j.aeue.2017.06.011.

[27] M. Khanra, J. Pal, K. Biswas, Rational approximation and analog realization of fractional order differentiator, Asian J. Control. 15 (2013) 723–735, https://doi.org/10.1002/asjc.565.

[28] A. Kartci, A. Agambayev, M. Farhat, N. Herencsar, L. Brancik, H. Bagci, K.N. Salama, Synthesis and optimization of fractional-order elements using a genetic algorithm, IEEE Access 7 (2019) 80233–80246, https://doi.org/10.1109/ACCESS.2019.2923166.

[29] B.T. Krishna, Realization of fractance device using fifth order approximation, Commun. Appl. Electron. 7 (2020) 1–5, https://doi.org/10.5120/cae2020652869.

[30] G. Tsirimokou, A. Kartci, J. Koton, N. Herencsar, C. Psychalinos, Comparative study of discrete component realizations of fractional-order capacitor and inductor active emulators, J. Circuits, Syst. Comput. 27 (2018), https://doi.org/10.1142/S0218126618501700.

[31] B.T. Krishna, Studies on fractional order differentiators and integrators: A survey, Signal Processing. 91 (3) (2011) 386–426, https://doi.org/10.1016/j.sigpro.2010.06.022.

[32] Y. Chen, I. Petráš, D. Xue, Fractional order control-a tutorial, in: 2009 Am. Control Conf., Hyatt Regency Riverfront, St. Louis, MO, USA, 2009: pp. 1397–1411.

[33] I. Podlubny, I. Petráš, B.M. Vinagre, P. O'Leary, L. Dorčák, Analogue realizations of fractional order controllers, Nonlinear Dyn. 29 (2002) 281–296.

[34] A.K. Mahmood, S.A.R. Saleh, Realization of fractional order differentiatior by analog electronic circuit, Int. J. Adv. Eng. Technol. 8 (2015) 1939–1951.

[35] T. Freeborn, B. Maundy, A.S. Elwakil, Approximated fractional order Chebyshev lowpass filters, Math. Probl. Eng. 2015 (2015) 7, https://doi.org/10.1155/2015/832468.

[36] B.C. Lim, J.E. Jang, J. Mao, J. Kim, M. Horowitz, Digital analog design: enabling mixed-signal system validation, IEEE Des. Test. 32 (2015) 44–52, https://doi.org/10.1109/MDAT.2014.2361718.

[37] A. Tepljakov, E. Petlenkov, J. Belikov, Efficient analog implementations of fractional-order controllers, in: Proc. 2013 14th Int. Carpathian Control Conf. ICCC 2013. (2013) 377–382. 10.1109/CarpathianCC.2013.6560573.

[38] A. Yüce, N. Tan, Electronic realisation technique for fractional order integrators, J. Eng. 2020 (5) (2020) 157–167, https://doi.org/10.1049/joe.2019.1024.

[39] C. Muñiz-Montero, L.V. García-Jiménez, L.A. Sánchez-Gaspariano, C. Sánchez-López, V.R. González-Díaz, E. Tlelo-Cuautle, New alternatives for analog implementation of fractional-order integrators, differentiators and PID controllers based on integer-order integrators, Nonlinear Dyn. 90 (1) (2017) 241–256, https://doi.org/10.1007/s11071-017-3658-z.

[40] R. Sotner, O. Domansky, J. Jerabek, N. Herencsar, J. Petrzela, D. Andriukaitis, Integer-and fractional-order integral and derivative two-port summations: practical design considerations, Appl. Sci. 10 (2020) 1–25, https://doi.org/10.3390/app10010054.

[41] R. Sotner, J. Jerabek, A. Kartci, O. Domansky, N. Herencsar, V. Kledrowetz, B.B. Alagoz, C. Yeroglu, Electronically reconfigurable two-path fractional-order PI/D controller employing constant phase blocks based on bilinear segments using CMOS modified current differencing unit, Microelectron. J. 86 (2019) 114–129, https://doi.org/10.1016/j.mejo.2019.03.003.

[42] I. Dimeas, I. Petras, C. Psychalinos, New analog implementation technique for fractional-order controller: A DC motor control, AEU - Int. J. Electron. Commun. 78 (2017) 192–200, https://doi.org/10.1016/j.aeue.2017.03.010.

[43] S. Kapoulea, C. Psychalinos, A.S. Elwakil, Single active element implementation of fractional-order differentiators and integrators, AEU - Int. J. Electron. Commun. 97 (2018) 6–15, https://doi.org/10.1016/j.aeue.2018.09.046.

[44] P. Bertsias, C. Psychalinos, B.J. Maundy, A.S. Elwakil, A.G. Radwan, Partial fraction expansion–based realizations of fractional-order differentiators and integrators using active filters, Int. J. Circuit Theory Appl. 47 (4) (2019) 513–531, https://doi.org/10.1002/cta.2598.

[45] S. Kapoulea, C. Psychalinos, A.S. Elwakil, S.H. HosseinNia, Realizations of fractional-order PID loop-shaping controller for mechatronic applications, Integration 80 (2021) 5–12, https://doi.org/10.1016/j.vlsi.2021.04.009.

[46] F.N. Deniz, B.B. Alagoz, N. Tan, M. Koseoglu, Revisiting four approximation methods for fractional order transfer function implementations: Stability preservation, time and frequency response matching analyses, Annu. Rev. Control. 49 (2020) 239–257, https://doi.org/10.1016/j.arcontrol.2020.03.003.

[47] V. Vinagre, B.M. Podlubny, I. Hernández, A. Feliu, Some approximations of fractional order operators used in control theory and applications, Fract. Calc. Appl. Anal. 3 (2000) 231–248.

[48] A. Oustaloup, F. Levron, B. Mathieu, F.M. Nanot, Frequency-band complex noninteger differentiator: Characterization and synthesis, IEEE Trans. Circuits Syst. I Fundam. Theory Appl. 47 (2000) 25–39, https://doi.org/10.1109/81.817385.

[49] A.N. Khovanskii, The Application of Continued Fractions and Their Generalizations to Problems in Approximation Theory, Noordhoff, Groningen, The Netherlands, 1963. 10.1017/s0008439500032033.

[50] K. Matsuda, H. Fujii, H(infinity) optimized wave-absorbing control - Analytical and experimental results, J. Guid. Control. Dyn. 16 (6) (1993) 1146–1153, https://doi.org/10.2514/3.21139.

[51] F.N. Deniz, Modelling and Control Applications in Fractional Order Systems, Inonu University, 2017.
[52] F.N. Deniz, B.B. Alagoz, N. Tan, D.P. Atherton, An integer order approximation method based on stability boundary locus for fractional order derivative/integrator operators, ISA Trans. 62 (2016) 154–163, https://doi.org/10.1016/j.isatra.2016.01.020.
[53] T.T. Hartley, C.F. Lorenzo, Dynamics and control of initialized fractional-order systems, Nonlinear Dyn. 29 (2002) 201–233, https://doi.org/10.1023/A:1016534921583.
[54] National Instruments, Electronics Workbench Group. NI Multisim14.1, Available: http://www.ni.com/multisim/, (2017).
[55] MATLAB Release 2020b, The MathWorks, Inc., Natick, Massachusetts, United States, (2020).
[56] E.A. Gonzalez, Ľ. Dorčák, C.A. Monje, J. Valsa, F.S. Caluyo, I. Petráš, Conceptual design of a selectable fractional-order differentiator for industrial applications, Fract. Calc. Appl. Anal. 17 (2014) 697–716, https://doi.org/10.2478/s13540-014-0195-z.